These observations clearly showed that although two types of active species are formed initially, the carboxylate anions are eventually responsible for most of the growth of macromolecules in the anionic polymerization of β-propiolactone.

Similar results were obtained in the polymerization of β-butyrolactone **2** initiated by potassium anions. This unexpected behavior of β-butyrolactone, which was believed not to polymerize by anionic initiators but rather by coordinative ones,[12,13] is possibly due to the very fast initiation by potassium anions and the complexation of counterions by crown ether.

The formation of an enolate in the initiation step of this polymerization (Scheme II) might suggest that both carbanion and enolate sites of this intermediate are able to react with the next lactone molecule. However, the $^1H$ NMR spectrum (Figure 1) indicates clearly that the polymer exhibits acetate and not β-diketo end groups. Moreover, the polymerization of β-propiolactone by the enolate of potassium acetate showed that the polymerization reaction is much faster than possible Claisen ester condensation.[14] Thus, the enolate of potassium acetate as well as the intermediate enolate carbanion formed in the initiation step of the β-lactone polymerization by potassium anions react regioselectively with β-propiolactones.

The results of this work confirm previous observations that in the anionic[15] as well as cationic[16] polymerization of heterocycles, two different mechanisms may operate simultaneously and thus indicate the existence of a more complex process of ionic ring-opening polymerization than was suggested previously.

## Conclusions

These results indicate that in the polymerization of β-lactones by potassium anions, the C–C cleavage at the α to β position in a β-lactone molecule takes place in the initiation step. Then, both alkyl–oxygen and acyl–oxygen bond cleavage occur to form carboxylate and alkoxide anions. Finally, the alkoxide active species disappear, and carboxylate anions are responsible for most of the polymer chain growth.

**Registry No.** $K^-$, 19128-96-2; $H_3CCO_2(CH_2)_3CO_2H$, 26976-72-7; $H_3CCO_2CH_2CO(CH_2)_2OH$, 119908-63-3; β-propiolactone, 57-57-8.

## References and Notes


(1) Jedliński, Z.; Kowalczuk, M.; Grobelny, Z.; Stolarzewicz, A. *Makromol. Chem., Rapid Commun.* **1983**, *4*, 355.
(2) Jedliński, Z.; Kowalczuk, M.; Kurcok, P.; Brzoskowska, L.; Franek, J. *Makromol. Chem.* **1987**, *188*, 1575.
(3) Jedliński, Z.; Kurcok, P.; Kowalczuk, M. *Macromolecules* **1985**, *18*, 2679.
(4) Jedliński, Z. Proceedings of the IUPAC Congress, Sophia, 1987.
(5) Shiota, T.; Goto, Y.; Hayashi, H. *J. Appl. Polym. Sci.* **1963**, *11*, 753.
(6) Weissberger, W. *Organic Solvents*; Wiley-Interscience: New York, 1974; p 704.
(7) Jedliński, Z.; Stolarzewicz, A.; Grobelny, Z.; Szwarc, M. *J. Phys. Chem.* **1984**, *88*, 6094.
(8) Kim, Ch.; Dodge, A.; Lan, S.; Kawasaki, A. *Anal. Chem.* **1982**, *54*, 232.
(9) Johns, D. B.; Lenz, R. W. In *Ring Opening Polymerization*; Ivin, K. J., Saegusa, T., Eds.; Elsevier: New York, 1984; Vol. 1, p 461.
(10) Yamashita, Y.; Tsuda, T.; Ishida, H.; Uchikawa, A.; Kuriyama, Y. *Makromol. Chem.* **1968**, *113*, 139.
(11) Yamashita, Y.; Hane, T. *J. Polym. Sci., Polym. Chem. Ed.* **1973**, *11*, 425.
(12) Yasuda, T.; Aida, T.; Inoue, S. *Makromol. Chem., Rapid Commun.* **1982**, *3*, 585.
(13) Kricheldorf, H.; Berl, M.; Scharnagl, N. *Macromolecules* **1988**, *21*, 286.
(14) The enolate of potassium acetate was prepared in THF solution from potassium acetate and potassium naphthalenide according to Angelo et al.[17] The polymerization of β-propiolactone in the presence of the above initiator was conducted under the conditions used for the polymerization with potassium anions. After the polymerization was terminated, the polymer was precipitated in methanol, filtered, and dried under high vacuum. The polyester was subsequently analyzed by $^1H$ NMR and VPO techniques. The $^1H$ NMR spectrum of the polyester ($M_n$ = 1200) revealed that besides the signals of the protons of the polyester chain ($\delta$ = 2.7 and $\delta$ = 4.3 ppm) only the singlet of the acetate end group ($\delta$ = 2.1 ppm) was observed, which indicates that the polymerization reaction proceeds much faster than Claisen ester condensation.
(15) Jedliński, Z.; Kasperczyk, J.; Dworak, A.; Matuszewska, B. *Makromol. Chem.* **1982**, *183*, 587.
(16) Kricheldorf, H. R.; Dunsing, R.; Serra, A. *Macromolecules* **1987**, *20*, 2050.
(17) Normant, H.; Angelo, B. *Bull. Soc. Chim. Fr.* **1962**, 810.


# Morphological Study of Supported Chromium Polymerization Catalysts. 2. Initial Stages of Polymerization


**Edward L. Weist, Ahmed H. Ali, Bharat G. Naik, and Wm. Curtis Conner***

*Department of Chemical Engineering, University of Massachusetts, Amherst, Massachusetts 01003.*


*Received October 17, 1988; Revised Manuscript Received January 16, 1989*



ABSTRACT: The changes in morphology due to the formation of polyethylene in the pores of three silica-supported, chromium oxide catalysts were followed by using mercury porosimetry and electron microscopy. Ethylene polymerization from 0.1 to 20 g of polymer/g of catalyst was carried out from the gas phase in a fluid bed reactor at 1-atm total pressure with a nitrogen diluent. A catalyst with 1.7 $cm^3/g$ pore volume fragmented due to the formation of polymer in the pores and thereby maintained an open structure. Catalysts containing 1.1 and 2.3 $cm^3/g$ pore volume did not fragment extensively, and the product polymer congested the pores and impeded the continued polymerization. Total pore volume and pore size are not the only controlling factors in the fracturing process. Mercury porosimetry showed that fracture of the 1.7 $cm^3/g$ catalyst started after a polymer yield of just 0.4 $g_{PE}/g_{cat}$, maintaining monomer access to the active sites. The 0.1–1-μm catalyst fragments contained a pore microstructure much like that of the starting material, thus demonstrating how the pore structure of the original catalyst particles may influence the polymerization process after fragmentation is complete.


## Introduction

The morphology of supported, ethylene polymerization catalysts has a great influence on the polymerization process. Several studies have shown that chromium and titanium deposited on supports with greater initial pore volume and larger average pore sizes exhibit greater po-

0024-9297/89/2222-3244$01.50/0 

lymerization activity.[1-4] It has also been shown that chromium oxide deposited on silica gels of higher pore volume produces a polymer of lower molecular weight, even though the formation of the polyethylene in the pores of the catalyst fractures the support to fragments more than 3 orders of magnitude smaller than the original catalyst during the initial stages of reaction.[4] Thus, not only does the morphology of the support influence the reaction, but it also changes during the reaction. Few prior studies have attempted to understand how the support influences the polymerization process.

McDaniel studied the fracturing of silica-based, polymerization catalyst supports by removing the polymer product in a muffle furnace at 650 °C.[2] The slurry polymerization was conducted in a stirred batch reactor. Nitrogen adsorption/desorption was used to characterize the fragments of the most active catalyst after polymerization. He demonstrated that the large increase in the pore volume due to fragmentation occurred in pores larger than the 60-nm-diameter pores measurable by this technique. He concluded that the fracture occurred along pores larger than 60 nm in diameter. Recently, McDaniel published a similar study using mercury porosimetry (a better technique for the evaluation of the larger pores) to assess the pore structure of the catalyst and fragments after polyethylene removal.[4] He found a correlation between the polymerization activity and the pore volume in pores between 10 and 100 nm in diameter as determined by mercury intrusion porosimetry. After removing the polymer, it was found that the catalyst fragments contained more pore volume in pores greater than 30 nm in diameter compared to the original catalyst, and McDaniel concluded that the fracture occurred along these pores during this process.

In the first paper of this series, we reported the changes that occurred in the pore structure of three chromium oxide–silica catalysts due to the high-temperature activation procedure.[5] It was found that the pretreatment of the most active catalyst resulted in a bimodal distribution of pores (and constrictions). In this work, the changes in the pore structure of the catalyst due to polymer formation are addressed. The reaction was conducted in a fluidized bed at 1-atm total pressure with a nitrogen diluent. Mercury porosimetry of the partially polymerized and fragmented catalysts reveal where the polymer is forming in the catalyst and which pores may play an important role in the process. Porosimetry of the catalyst fragments after polymer removal indicate which pores were most affected by the polymer formation and which pores are necessary for fracture and fragmentation.

## Experimental Section

**Catalysts.** The catalysts, supplied by the Phillips Chemical Co., were the same as those in our prior studies (and were presumably similar to those employed by McDaniel[2,4]): 1% by weight chromium deposited on three silica supports of nominal pore volumes of 1.1–1.2, 1.6–1.7, and 2.2–2.3 $cm^3/g$.[5] In addition to differences in pore volume, the supports were prepared by different procedures and possessed different particle shapes; however, these factors were not investigated in these studies. Before activation and reaction, the catalyst particles were screened in 63–125-$\mu$m sieves. The sieved catalyst (0.3–0.7 g) was activated for reaction in situ in a 20-mm-diameter fluid bed by the following procedure: (1) drying in nitrogen at 150 °C for 1 h; (2) heating at a rate of 200 °C/h in oxygen to 800 °C; (3) calcination in oxygen at 800 °C for 5 h; (4) cooling in oxygen to 400 °C over a 1-h period; (5) purging with nitrogen for 10 min at 400 °C; (6) reduction in carbon monoxide at 400 °C for 1 h; (7) cooling to 100 °C in nitrogen over a 1-h period. The activity that results from this procedure is found to exceed 10 $g_{PE}/(g_{cat}\cdot atm\cdot h)$ as was also found in our prior studies.[5] This activity compares favorably with that published by Phillips and employs their optimum activation procedure.[2,4]

The high-temperature activation process caused changes in the pore structure of the catalysts due to a sintering of the silica.[5] In addition to variation in the nominal pore volume, the three catalysts also contained different pore-size distributions as determined by mercury porosimetry: the 1.1 $cm^3/g$ catalyst contained most of its pore volume accessed through 9–12-nm-diameter throats; the 1.7 $cm^3/g$ catalyst also had throats in this size range, in addition to a significant amount of pore volume accessed through throats larger than 20-nm diameter; 2.3 $cm^3/g$ catalyst had most of its pore volume accessed through throats larger than 20-nm diameter with a small amount accessed through throats of 4.5–5-nm diameter.[5]

**Polymerization.** The polymerization of ethylene was carried out in the same reactor immediately after cooling the catalyst bed to 100 °C in flowing nitrogen following the prereduction by carbon monoxide. Because the addition of monomer at the active site is so exothermic (24 kcal/mol[6]), the polymerization had to be performed with a diluent. A solid diluent was not used due to the difficulty in removing the product from the inert substances. Therefore, the reaction was carried out using a gaseous diluent, nitrogen. The exothermicity of the reaction required that the monomer be introduced in small concentrations initially and then increased as the growing polyethylene acted as a source for dissipation of the heat of reaction. Thus, two schemes were used to introduce monomer to the catalyst bed during the initial stages of the reaction.

In the first scheme, ethylene was bled into a 750 $cm^3/min$ (STP) nitrogen stream so that the monomer concentration was 1% for the first 5 min. The ethylene concentration was then slowly increased to 10% in another 15 min and to 40% in another 20 min. During this period, the total gas flow rate was increased to maintain fluidization of the growing catalyst/polymer particles. In the second scheme, pulses of ethylene were added to a 670 $cm^3/min$ (STP) nitrogen flow for 2 s every 10 s so that the stream entering the reactor contained 40% monomer. With this method, the feed stream could be switch to a constant 40% monomer after 10 min of pulses. With either method, the temperature, as measured by a chromel–alumel thermocouple in the catalyst bed, was within ±2 °C of the 100 °C reaction temperature during these initial stages. The thermocouple could be adjusted to any position in the bed during the reaction, and no temperature nonuniformities were observed.

The polymerization continued for a predetermined length of time, at which point the catalyst bed was starved of ethylene and cooled to room temperature. The polymer yield was determined by analyzing the product for carbon and hydrogen content. Polymer yields up to 20 g of polyethylene/g of catalyst ($g_{PE}/g_{cat}$) could be determined by this method.

**Polymer Removal.** To study the pore structure of the catalyst fragments, the polyethylene was removed from the chromium–silica catalyst by two methods: dissolution by a solvent and/or oxygen plasma ashing. Polymer extraction by 1,2,4-trichlorobenzene was done using a Soxhlet apparatus with a 4-$\mu$m extraction thimble. The temperature of the extraction was held at 140 °C for 6 h, then increased slowly to 190 °C over a 6-h period, and held at this temperature for another 36 h. This procedure removed 95% of the polyethylene from the catalyst, with some polymer chains holding the fragments together. The remaining polymer was removed by ashing in a Paar Cool Plasma Asher, which generates oxygen plasma at 2–4-mbar pressure by radio frequency excitation. By this method, the polyethylene could be gently burned away over a 12–24-h period. Further, we found no evidence that any of the catalyst was lost during these processes.

Mercury porosimetry and microscopy showed that the above procedures affected neither porosity or structure of the unreacted catalyst particle nor that of a catalyst which had been filled with *n*-dodecane.

**Mercury Porosimetry.** The pore structures of the catalysts were characterized by using a Quantachrome scanning mercury porosimeter capable of measuring pores sizes from 4 to $10^4$ nm in diameter by applying pressure up to 60 000 psi. The catalyst samples were first outgassed at 150 °C for 1 h at less than $10^{-4}$ Torr in a vacuum system for BET surface area determination and

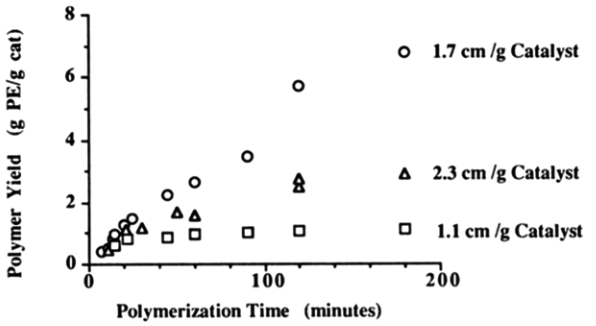


**Figure 1.** Polyethylene growth on the chromium oxide–silica catalysts: 100 °C, 10% ethylene concentration.

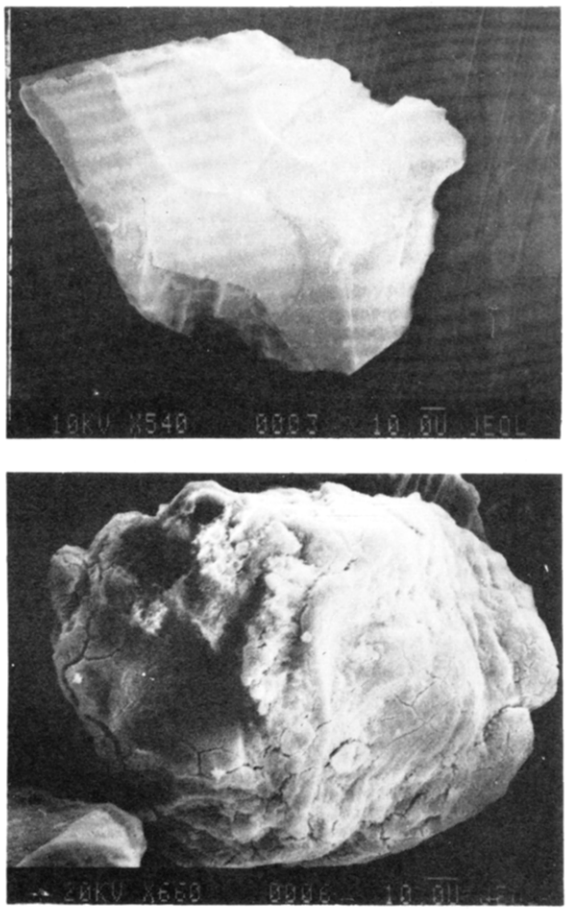

**Figure 2.** Electron micrographs of the 1.1 $cm^3/g$ catalyst before and after polymerization. The top picture is of the freshly activated catalyst and the bottom picture represents a yield of 2 $g_{PE}/g_{cat}$.

then transferred to the porosimetry cell. Before mercury intrusion, the catalysts were outgassed at less than $10^{-1}$ Torr for 15 min at room temperature. The void dimensions were related to the applied pressure by the Washburn equation: $Pd = 4\gamma \cos\theta$, where $P$ is the applied pressure, $d$ is the diameter of the pore, $\gamma$ is the surface tension of the mercury (484 dyn/cm), and $\theta$ is the angle of contact between the mercury and the walls of the catalyst (assumed to be 140°).

When using mercury porosimetry for the evaluation of catalyst pore structure, it is essential to understand the information given by the intrusion and retraction branches of the hysteresis loop. A "pore-throat" structural model based on agglomerated spheres has been developed to explain hysteresis and mercury retention.[7] The mercury intrusion process is controlled by the size of the constrictions, or "throats", in the pore network, while the mercury retraction process is controlled by the size of the opening, or "pores". Therefore mercury intrusion measures the size of the throat along with the volume of the pore behind it. A Monte Carlo simulation based on this model showed a relationship between

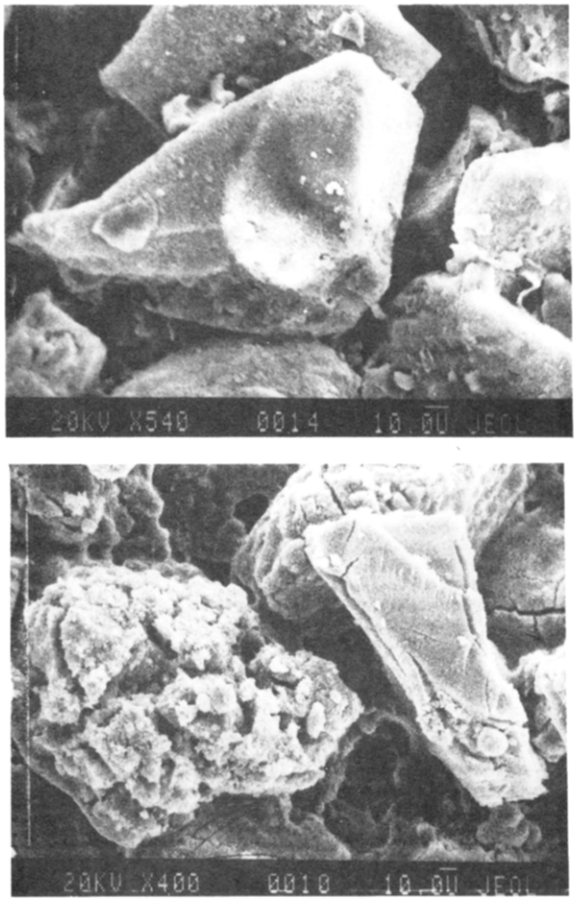

**Figure 3.** Electron micrographs of the 2.3 $cm^3/g$ catalyst before and after polymerization. The top picture is of the freshly activated catalyst and the bottom picture represents a yield of 5 $g_{PE}/g_{cat}$.

mercury retention and particle size and connectivity (degree of branching in the void network).[8]

## Results and Discussion

We will first examine the changes in the pore structure due to the formation of polymer within the catalyst pores. These changes will be compared to the pore structure of the active catalyst. We will then examine the changes in the pore structure that are evident after the product polymer has been removed from the product solid.

**Polymer Growth.** Of the three chromium–silica catalysts used in this study, only the catalyst with 1.7 $cm^3/g$ pore volume exhibited constant polymerization activity in the fluid bed reactor under these conditions. Figure 1 shows the polymer yield in grams of polyethylene per gram of catalyst ($g_{PE}/g_{cat}$) for the three catalysts versus time of exposure to a 10% ethylene in nitrogen feed at 100 °C. The formation of polyethylene in the 1.1 and 2.3 $cm^3/g$ catalysts slowed appreciably after formation of approximately 1 and 2.5 $g_{PE}/g_{cat}$, respectively. Assuming a polymer density of 0.94 $g/cm^3$, these yields correspond approximately to the amount of polyethylene needed to fill the available pore volume of the supports. The electron micrographs in Figures 2 show no evidence for fracture in the 1.1 $cm^3/g$ catalyst. In Figure 3 some large cracks are evident in the 2.3 $cm^3/g$ catalyst. In each case enough polyethylene had been produced to fill twice the available pore volume of the respective supports. The 2.3 $cm^3/g$ catalyst support seems to have fragmented into plates of 10–20 $\mu m$ in size. On the other hand, large cracks appear very early in the 1.7 $cm^3/g$ catalyst support as shown in Figure 4, and, after the formation of enough polymer to

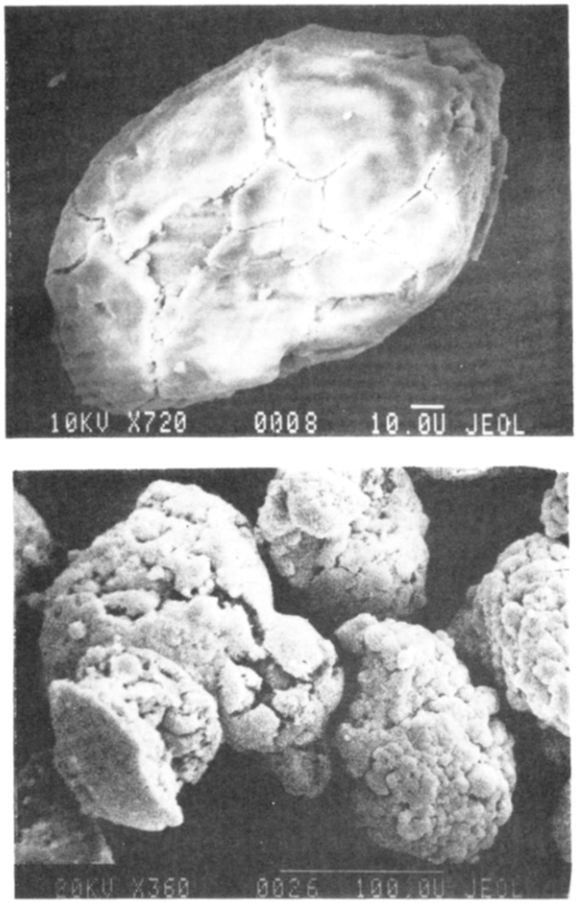


**Figure 4.** Electron micrographs of the 1.7 $cm^3/g$ catalyst before and after polymerization. The top picture is of the freshly activated catalyst and the bottom picture represents a yield of 4 $g_{PE}/g_{cat}$.

fill twice the available pore volume, the particles appear to consist of an agglomeration of polymer coated catalyst fragments.

Thus, the sustained activity of the 1.7 $cm^3/g$ catalyst was due to the fracture and fragmentation of the support, maintaining a network of pores in the particles that facilitated the transport of the monomer to the active site. The decrease in polymerization activity of the other two catalysts was due to the slow diffusion of the monomer through the polyethylene, which was clogging the initial pore structure. The transport limitations were especially severe in this reactor because of the small driving force for diffusion due to the low monomer concentration in the gas phase. Higher yields were achieved only by raising the ethylene concentration to 40 or 100% and allowing the reaction to continue for several hours. The low activity of the 2.3 $cm^3/g$ catalyst was surprising in light of the general trend of increasing activity with increasing pore volume and pore size. Indeed, we have evidence that polymerization at higher pressures (to 30 bar) can result in higher polymer yields than at these pressures (<1-bar monomer pressure) for both the 1.1 and 2.3 $cm^3/g$ catalysts.[9]

To determine the regions of the catalyst in which the polymer was forming, the progressive pore filling of the support with polyethylene was followed by using mercury porosimetry up to the point where the polymer completely filled the void space. At higher yields, compression of the polyethylene made the interpretation of the results difficult. The porosimetry plots in Figure 5 show that there was a linear decrease in accessible pore volume of the 1.1 $cm^3/g$ catalyst with the amount of polyethylene formed.

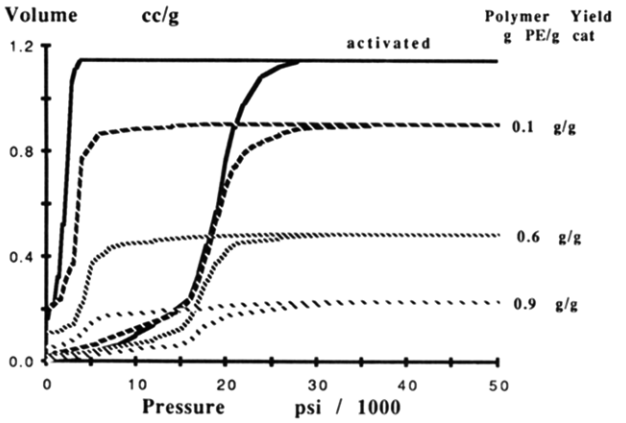


**Figure 5.** Effect of polyethylene formation on the porosimetry plot of the 1.1 $cm^3/g$ catalyst with polymer.

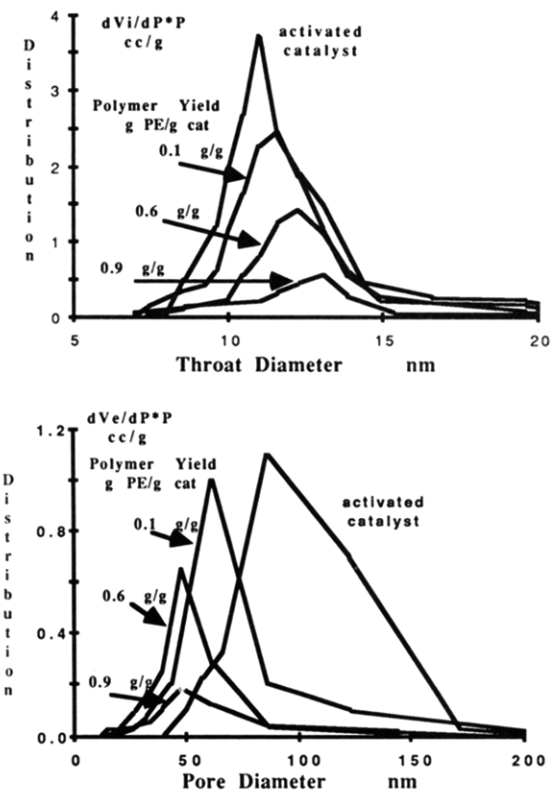


**Figure 6.** Effect of polyethylene formation on the throat- and pore-size distributions of the 1.1 $cm^3/g$ catalyst with polymer.

It should be noted that for each of the sets of porosimetry data the lower curve represents the intrusion measurement (as mercury pressure is increased) and the upper curves represent the retraction curves (as pressure is decreased). There is a noticeable change in the pressures over which retraction occurs (i.e., the distribution of pore size distributions is shifting), but there is little change in the pore (constriction) size distribution from the intrusion curve. This is better illustrated by the distributions shown in Figure 6. The center of the throat size distribution as measured by mercury intrusion shifted to slightly larger dimensions, indicating that the smallest throats were blocked by the formation of polyethylene first. As expected, the pore-size distribution from the retraction curve shows that the size of the openings in the support decreased as the polymer formed. Thus, in the absence of fracture, the polyethylene formed in the openings (pores) of the catalyst where the accessible chromium surface exists. As the formation of polymer completely filled some

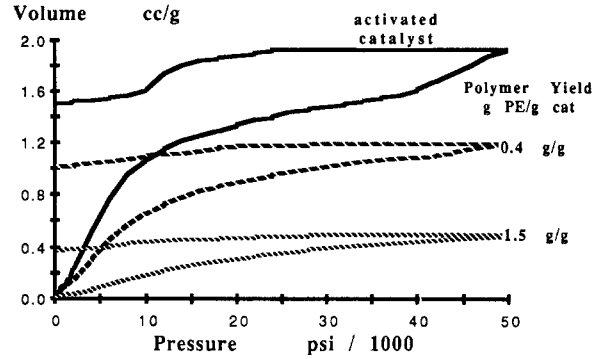


**Figure 7.** Effect of polyethylene formation on the throat- and pore-size distributions of the 2.3 $cm^3/g$ catalyst with polymer.

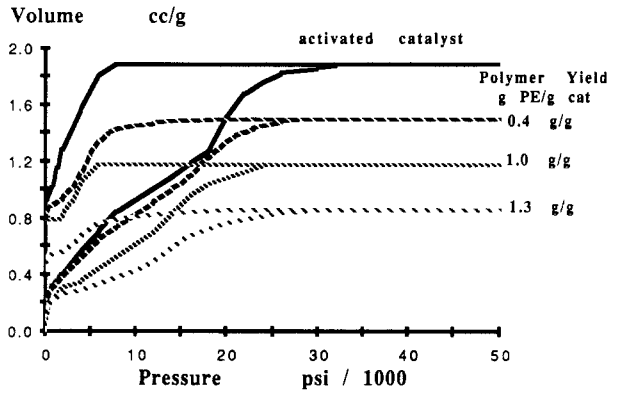


**Figure 8.** Effect of polyethylene formation on the porosimetry plot of the 1.7 $cm^3/g$ catalyst with polymer.

pores, the smallest throats were blocked by the polymer first.

The formation of polyethylene in the 2.3 $cm^3/g$ catalyst, the other catalyst that did not fracture extensively, affected the pore structure as measured by mercury porosimetry differently than in the preceding case. Figure 7 shows that the formation of polyethylene effected a rapid decrease in the accessible pore volume. After a polymer yield of just 0.4 $g_{PE}/g_{cat}$, the pore volume of the catalyst decreased more than 40%, and the porosimetry plot and the distributions are essentially featureless. Polyethylene formation has blocked some of the pores in this support, occluding some of the initial pore volume.

Figure 8 shows that the formation of polymer in the 1.7 $cm^3/g$ catalyst, which fractured extensively even at these low yields, did not decrease the accessible pore volume in a linear fashion as it did in the 1.1 $cm^3/g$ catalyst. The void-size distributions in Figure 9 show that the fracture and fragmentation of this catalyst support maintained an open porous network in the particle. There was some blocking of the smaller throats as seen in the 1.1 $cm^3/g$ catalyst but very little change in the center of the pore-size distribution given by mercury retraction after a polymer yield of 0.4 $g_{PE}/g_{cat}$. As more polymer is formed, the pores do not decrease in dimensions since the whole particle is expanding to accommodate the growing polymer. This indicates that the fracture and fragmentation of this catalyst support has already commenced even at these low yields.

**Catalyst Fragments.** The pore structures of the catalyst and catalyst fragments remaining after removal of the polymer were evaluated to identify the pores that were most affected by the polymer formation and, thus, to infer which pores were responsible for the fracture of the support. As expected, there was no change in the pore structure of the catalysts that did not fracture extensively during the reaction. Figures 10 and 11 show that the pore structures of the 1.1 and 2.3 $cm^3/g$ catalyst supports were

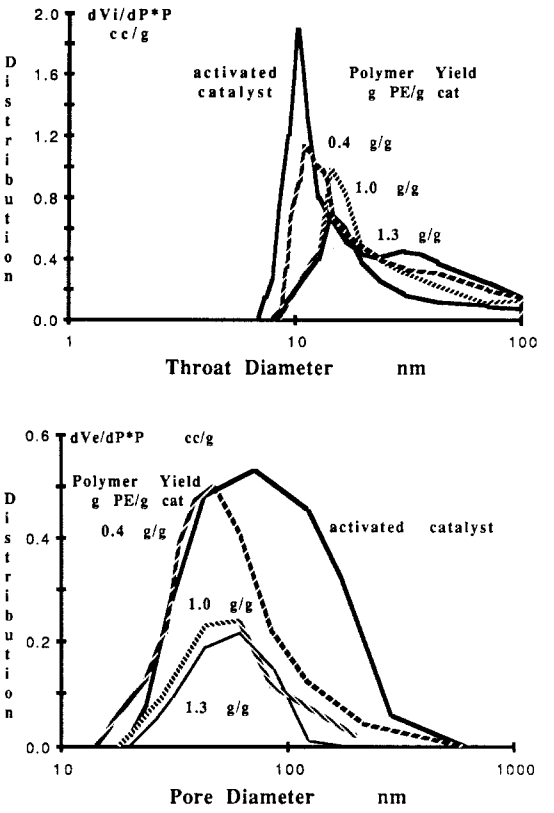


**Figure 9.** Effect of polyethylene formation on the throat- and pore-size distributions of the 1.7 $cm^3/g$ catalyst with polymer.

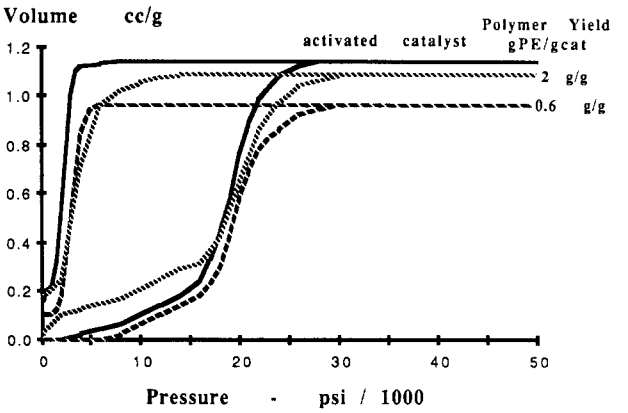


**Figure 10.** Effect of polyethylene formation on the porosimetry plot of the 1.1 $cm^3/g$ catalyst fragments after polymer removal.

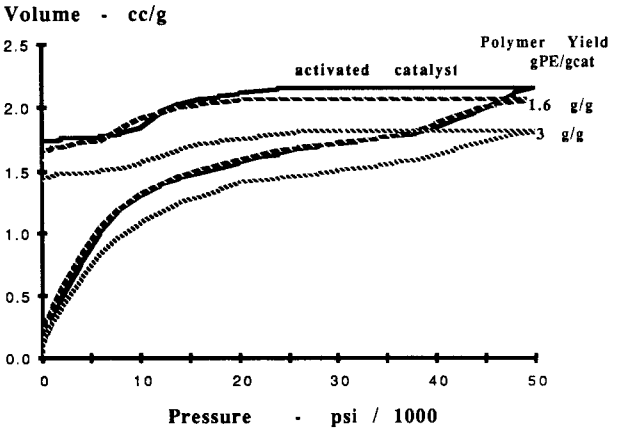


**Figure 11.** Effect of polyethylene formation on the porosimetry plot of the 2.3 $cm^3/g$ catalyst fragments after polymer removal.

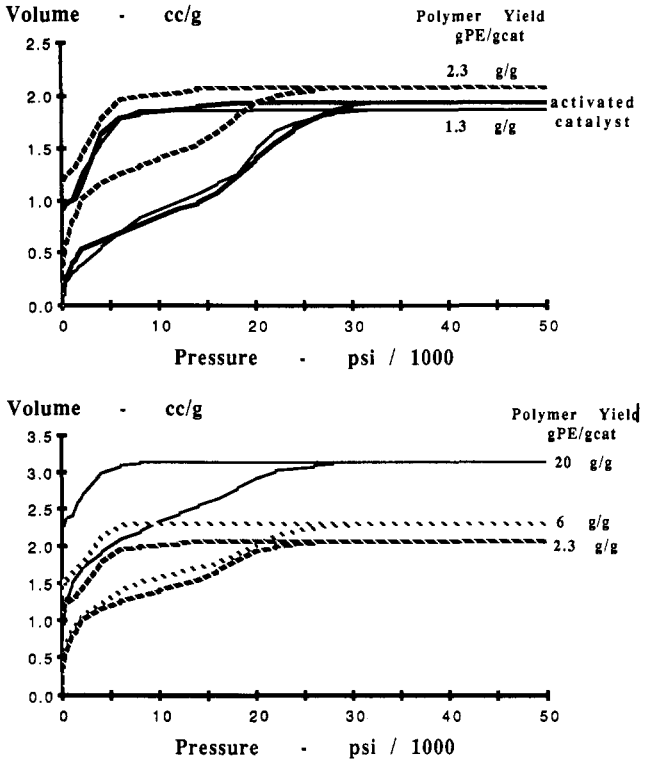


**Figure 12.** Effect of polyethylene formation on the porosimetry plot of the 1.7 $cm^3/g$ catalyst fragments after polymer removal.

basically unaffected by the polymer formation (after polymer removal), as was the macrostructure seen in the electron micrographs of the catalyst/polymer particles in Figures 2 and 3. The fragmentation of the 2.3 $cm^3/g$ catalyst into the 10-$\mu$m plates, inferred from the microscopy, is not expected to have a profound effect on the specific porosity as measured by mercury porosimetry.

Likewise, there was little change in the pore structure of the polymer free product for the 1.7 $cm^3/g$ catalyst support up to a polymer yield that corresponds to a complete filling of the pores. However, at higher yields there are noticeable changes in the pore structure. Figure 12 shows that there was an increase in the pore volume accessed through throats larger than 100-nm diameter (i.e., those measured below 2000 psig mercury pressure), while neither the throat sizes smaller than 100 nm in diameter nor the retraction curve changed. Thus, the mesoporous structure of the catalyst support remained the same even after a polymer yield of 20 $g_{PE}/g_{cat}$ and fragmentation to less than 1 $\mu$m in size. Complete fragmentation and separation would decrease the specific intraparticle pore volume slightly if the initial pore structure provides the primary pathways for fragmentation. The increase in pore volume as determined from the mercury porosimetry experiments was due to compression of the catalyst fragments and filling of the spaces between the fragments by the mercury in the porosimetry cell. When the ashed fragments were compressed to near the original apparent bulk density of the starting material, the increase in the pore volume accessed through throats larger than 100 nm in diameter completely disappeared. The mesoporous region remained constant during the polymerization process, showing that the fracture of the catalyst occurred along the largest pores. The pore space that would be formed by the agglomeration of spherical 0.1–1 $\mu$m particles should give intrusion at pressures corresponding to ~20–200 nm (~10 000–1000 psi Hg pressure) and retraction corresponding to ~50–500 nm (~4000–400 psi Hg pressure). These characteristics are evident in the data.

McDaniel also found an apparent increase in the pore volume of pores greater than 100 nm in diameter as determined from mercury intrusion.[4] The pore volume accessed by these larger throats for the catalyst, which initially contained 1.7 $cm^3/g$ pore volume, increased as the polymer yield increased from 12 to 1270 $g_{PE}/g_{cat}$.[4] Our study shows that significant fracture and fragmentation of this catalyst support has occurred by the time that just enough polyethylene has been formed to fill the pores. Moreover, we find that fracture is probably initiated at even lower yields.

## Conclusions

In a fluid bed reactor, the polymerization of ethylene in the pores of the three chromium oxide–silica catalysts was strongly dependent on the fragmentation of the catalyst. Only the catalyst containing an intermediate amount of pore volume (1.7 $cm^3/g$) fractured enough to maintain constant activity during exposure to a 10% ethylene feed for up to 3 h. The lack of extensive fracture and fragmentation in the other two catalysts (1.1 and 2.3 $cm^3/g$) with these reaction conditions resulted in a diffusion-limited reaction after formation of enough polyethylene to fill the pores of these catalysts. The diffusion limitations of the reaction were accentuated by the low monomer concentration in the reactor. These results show that the total pore volume and pore size are not the only controlling factors in catalyst fracture, but rather that the structure of the void network is the most significant factor. This is evidenced by the lack of complete fragmentation of the 2.3 $cm^3/g$ catalyst which has a larger pore volume and a similar distribution of pore dimension as found for the 1.7 $cm^3/g$ catalyst.

Mercury porosimetry of the 1.7 $cm^3/g$ catalyst support with polymer (polymer yield <1.7 $g_{PE}/g_{cat}$) showed that the fracture of the support maintained an open network of pores and throats in the particle which facilitated transport of the monomer to the active sites. The average pore size in this catalyst did not change substantially after a yield of 0.4 $g_{PE}/g_{cat}$, showing that the fracture starts early in the reaction (i.e., prior to the total filling of the catalyst void volume). New polymer forming on the catalyst internal surface forces the subparticles apart and does not just fill the pore space between fixed catalyst subparticles. A small shift is evident in the intrusion data due to accumulation of polymer at the constrictions in the void network. From mercury porosimetry of the catalyst fragments after removal of the polyethylene, the fragmentation of the catalyst was not evident until the formation of enough polymer to fill the pores of the support. Partial fragmentation would be difficult to detect as the measurement by porosimetry tends to recompact the sample. Extensive fragmentation was reflected in an apparent increase in the pore volume accessed through throats larger than 100 nm. This increase was due to compression of the fragments by the mercury and filling of the spaces between the fragments. The region of compression and intrusion confirm that the fragments are on the order of 0.1–1 $\mu$m.

The pore structure of the catalyst fragments is much like that of the original catalyst particles. Thus, the initial pore volume and pore size of the subparticles comprising the support are present in the final catalyst fragments and can influence the polymerization and resultant polymer product even after complete fragmentation, which occurs very early in the progress of the reaction.

We conclude that the nature of the porous network controls the fragmentation. Pore volume alone does not dictate the potential performance of a polymerization

catalyst, as implied in prior studies. The pore dimensions and the distribution of these within the void network can control fragmentation and thereby the performance. To facilitate continued polymerization, the network should not become unduly congested by the polymeric product. Fragmentation of the catalyst depends on several interrelated aspects of the solid catalyst. These may include (but are not restricted to) the void fraction, the distribution of void dimensions, the nature of the connection between subparticles and the pore structure of the subparticles, the rate of polymer formation (and related heat generation), and the associated chemistry of the active polymerization sites as influenced by the preparation and pretreatment of the catalytic system.

**Acknowledgment.** The National Science Foundation supported this work under NSF Grant CBT-85-15479. We thank Drs. Frederick Karol and Burkhard Wagner of Union Carbide Corp. for their helpful discussion and Union Carbide for supporting this work financially. Dr. Max McDaniel of Phillips Chemical Co. supplied the catalysts. We thank Dr. Ramon Barnes of the Chemistry Department for use of the oxygen plasma asher and Lou Raboin for his help with the electron microscopy.

**Registry No.** PE, 9002-88-4; chromium oxide, 11118-57-3.

## References and Notes

(1) Carrick, W. L.; Turbett, R. J.; Karol, F. J.; Karapinka, G. L.; Fox, A. S.; Johnson, R. N. *J. Polym. Sci., A-1* **1972**, *10*, 2609.
(2) McDaniel, M. P. *J. Polym. Sci., Polym. Chem. Ed.* **1981**, *19*, 1967.
(3) Munoz-Escalona, A.; Hernandez, J. G.; Gallardo, J. A. *J. Appl. Polym. Sci.* **1984**, *29*, 1187.
(4) McDaniel, M. P. In *Adv. Catal.* **1985**, *33*, 47.
(5) Weist, E. L.; Ali, A. H.; Conner, W. C. *Macromolecules* **1987**, *20*, 689.
(6) Hogan, J. P. In *Applied Industrial Catalysis*; Leach, B. E., Ed.; Academic Press: New York, 1983; Vol. 1, Chapter 6.
(7) Conner, W. C.; Lane, A. M.; Ng, K. M.; Goldblatt, M. *J. Catal.* **1983**, *83*, 336.
(8) Conner, W. C.; Lane, A. M. *J. Catal.* **1984**, *89*, 217.
(9) Webb, S.; Conner, W. C.; Laurence, R. L., unpublished results.

# Pseudopoly(amino acids): A Study of the Synthesis and Characterization of Poly(*trans*-4-hydroxy-*N*-acyl-L-proline esters)

**Heewon Yu Kwon† and Robert Langer***

*Department of Chemical Engineering, Massachusetts Institute of Technology, Cambridge, Massachusetts 02139.* *Received July 22, 1988; Revised Manuscript Received January 3, 1989*

ABSTRACT: The synthesis and characterization of polyesters derived from hydroxyproline (Hpr) were investigated. A series of new poly(*trans*-4-hydroxy-*N*-acyl-L-proline esters) were prepared in which the pendant acyl groups are ethanoyl (Ac), 2,2-dimethylpropanoyl (Piv), hexanoyl (Hex), decanoyl (Dec), tetradecanoyl (Myr), and hexadecanoyl (Pal). Weight average molecular weights ($M_w$) over 40 000 were obtained via ester interchange using 1 mol % titanium isopropoxide as a catalyst at 180 °C for 20–24 h. The different pendant groups on the monomers profoundly affect the polymerizability and the polymer properties. The molecular weight data obtained from gel permeation chromatography and vapor pressure osmometry suggest that these polymers assume a rodlet-like conformation in solution. When the length of the acyl group on the monomer increased, the molecular weight as well as the degree of polymerization increased. Differential scanning calorimetry analysis showed that poly(Ac-Hpr ester), poly(Piv-Hpr ester), poly(Hex-Hpr ester), and poly(Dec-Hpr ester) are amorphous, while poly(Myr-Hpr ester) and poly(Pal-Hpr ester) are semicrystalline. A declining trend in the glass transition temperatures of polymers was observed with increasing pendant chain length. However, it was reversed due to the side-chain crystallinity when the pendant chain length reached 14 carbons.

## Introduction

In continuing efforts to develop improved biomaterials, an approach for synthesizing a new class of poly(amino acids) was recently proposed.[1] These polymers, named "pseudopoly(amino acids)", are different from conventional poly(amino acids) in that the polymer backbone is formed by utilizing the side-chain functional groups on the monomeric α-L-amino acids or dipeptides. Such an approach offers the opportunity to create polymers from naturally occurring metabolites but without some of the potential disadvantages of conventional poly(amino acids) resulting from the repeating amide bonds (e.g., poor mechanical strength and enzymatic degradation).

To date, the syntheses of only three subclasses of these polymers have been reported:[1,2] poly[(benzyloxycarbonyl)tyrosyltyrosine hexyl ester iminocarbonate], poly[*trans*-4-hydroxy-1-(1-oxohexadecyl)-L-proline ester], and poly[(benzyloxycarbonyl)glutamylphenylalanine anhydride]. In addition to the flexibility of designing polymers possessing various properties attributable to the polymer main-chain bonds, this approach also offers another advantage—the modification at the level of amino acid termini. In pseudopoly(amino acids), either the amino group or the carboxyl group or both can be chemically modified or used as sites for covalent attachment of drugs or bioactive molecules. It has been shown that pendant groups can significantly alter the physical properties of polymers.[3] The effect of pendant groups on the polymerizability of pseudopoly(amino acids) and on the properties of these polymers has not been examined.

In this paper we first report a study examining factors affecting the molecular weight of poly(Pal-Hpr ester); specifically, temperature, amount of catalyst, reaction time, and type of catalysts were varied. Second, we describe the syntheses of several new poly(*trans*-4-hydroxy-*N*-acyl-L-proline esters) where the acyl group is systematically al-

* To whom correspondence should be addressed.
† Present address: Schering-Plough Corp., Kenilworth, NJ 07033

0024-9297/89/2222-3250$01.50/0 